

Important Notice to Authors

Attached is a PDF proof of your forthcoming article in Biomedical Optics Express. The article Manuscript ID is 415105. *No further processing of your paper will occur until we receive your response to this proof.*

Note: Excessive proof corrections submitted by the author can result in significant delays to publication. Please include only essential changes that might be needed to address any shortcomings noticed in the proof-preparation process.

Author Queries

Please answer these queries by marking the required corrections at the appropriate point in the text or referring to the relevant line number in your PDF proof.

Q1	The funding information for this article has been generated using the information you provided to OSA at the time of article submission. Please check it carefully. If any information needs to be corrected or added, please provide the full name of the funding organization/institution as provided in the Crossref Open Funder Registry (https://search.crossref.org/funding).
----	---

Other Items to Check

- Please note that the original manuscript has been converted to XML prior to the creation of the PDF proof, as described above. The PDF proof was generated using LaTeX for typesetting. The placement of your figures and tables may not be identical to your original paper.
- Please carefully check all key elements of the paper, particularly the equations and tabular data.
- Author list: Please make sure all authors are presented, in the appropriate order, and that all names are spelled correctly.
- If you need to supply new or replacement figures, please upload each figure as an individual PDF file at the desired final figure size. The figure must fit inside the margins of the manuscript, i.e., width no more than 5.3 inches (or 13.46 cm). Confirm the quality of the figures and upload the revised files when submitting proof corrections.

Model learning analysis of 3D optoacoustic mesoscopy images for the classification of atopic dermatitis

SOJEONG PARK,^{1,9} SHIER NEE SAW,^{1,2,9} XIUTING LI,^{3,9} MAHSA PAKNEZHAD,¹ DAVIDE COPPOLA,¹ U. S. DINISH,³ AMALINA BINITE EBRAHIM ATTIA,³ YIK WENG YEW,⁴ STEVEN TIEN GUAN THNG,⁴ HWEE KUAN LEE,^{1,5,6,7,8,10} AND MALINI OLIVO^{3,11}

¹Bioinformatics Institute, Agency of Science, Technology and Research, A*STAR, 30 Biopolis Street, #07-01 Matrix, 138671, Singapore

²Current address: Department of Artificial Intelligence, Faculty of Computer Science and Information Technology, University of Malaya, Malaysia

³Laboratory of Bio-Optical Imaging, Singapore Bioimaging Consortium, A*STAR, 11 Biopolis Way, 138667, Singapore

⁴National Skin Centre, 1 Mandalay, 308205, Singapore

⁵School of Computing, National University of Singapore, 13 Computing Drive, Singapore, 117417, Singapore

⁶Singapore Eye Research Institute (SERI), 11 Third Hospital Ave, Singapore, 168751, Singapore

⁷Image and Pervasive Access Laboratory (IPAL), 1 Fusionopolis Way, #21-01 Connexis (South Tower), 138632, Singapore

⁸Rehabilitation Research Institute of Singapore, 11 Mandalay Road #14-03, Clinical Sciences Building, 308232, Singapore

⁹Co-first authors

¹⁰leehk@bii.a-star.edu.sg

¹¹malini.olivo@sbic.a-star.edu.sg

Abstract: Atopic dermatitis (AD) is a skin inflammatory disease affecting 10% of the population worldwide. Raster-scanning optoacoustic mesoscopy (RSOM) has recently shown promise in dermatological imaging. We conducted a comprehensive analysis using three machine-learning models, random forest (RF), support vector machine (SVM), and convolutional neural network (CNN) for classifying healthy versus AD conditions, and sub-classifying different AD severities using RSOM images and clinical information. CNN model successfully differentiates healthy from AD patients with 97% accuracy. With limited data, RF achieved 65% accuracy in sub-classifying AD patients into mild versus moderate-severe cases. Identification of disease severities is vital in managing AD treatment.

© 2021 Optical Society of America under the terms of the [OSA Open Access Publishing Agreement](#)

1. Introduction

Atopic dermatitis (AD) is a chronic inflammatory skin disease with itch, inflammation and red rashes. The prevalence of AD is approximately 10% and it is more commonly seen in children, especially children under the age of five [1–3]. Nonetheless, an adult who suffers from AD tends to represent a more persistent and severe condition [4]. The cause of AD is unknown but there is evidence that suggests that genetic, allergic and environmental factors can be related to the development of AD [5–7].

The disease progression of AD can be variable and can proceed in three directions: (i) persistent AD, (ii) intermittent AD or (iii) improvement. It is therefore important to diagnose and prognosticate AD so that treatment can be tailored at each stage. Currently, many scoring systems are available to assess the severity of AD, such as Eczema Area Severity Index (EASI) and

52 Scoring Atopic Dermatitis (SCORAD), modified EASI (mEASI) and others [8–10]. However,
53 these scoring systems are semi-quantitative at the best as they are designed based on metrics
54 such as itchiness, redness and scale of the affected skin region, while others include the quality
55 of patients' life. In addition, these scoring systems are based on visual inspections and it has
56 been reported that visual skin assessments can only differentiate severities of AD in 25% of
57 cases when self-assessed by patients [11]. Furthermore, it requires experience and training for
58 clinicians to make visual assessments, subjecting these scoring systems to inter-rater variability
59 [12]. It is desirable to have a non-invasive objective scoring tool that reflects the true AD severity
60 throughout the therapeutic intervention and AD clinical trial, especially for mild and non-mild
61 severities.

62 Raster-Scanning Optoacoustic Mesoscopy (RSOM), first introduced in 2013, is an emerging
63 hybrid optical and ultrasound imaging technique that offers non-invasive, deep penetration
64 imaging and provides high-resolution images [13]. RSOM imaging provides deep skin structural
65 imaging up to 1–2 mm beneath the skin surface with high resolutions up to ~7 µm axial and ~30
66 µm lateral resolution [14]. With these resolutions, the vascular remodeling of the skin in various
67 clinical severities of AD can be detected by RSOM imaging [12,15,16]. Differential diagnosis
68 is thus critical to achieve accurate AD diagnosis [17]. Considerable efforts have been made to
69 explore the efficacy of RSOM in assessing skin inflammatory diseases. For example, skin-specific
70 metrics derived from RSOM such as total blood volume (TBV) and epidermis thickness (ET)
71 have shown a substantial difference between control and skin inflammatory conditions [,14, 18].
72 In another study by Li et al., the feasibility of using RSOM derived skin-specific metrics in
73 different skin phenotypes populations was investigated [19].

74 Machine learning models have shown significant success in the classification of skin disease
75 diagnosis using dermatological images of superficial skin conditions [20–27]. However, these
76 models have not been applied on RSOM images except for the work by Yew et al. [18]. In
77 the work by Yew et al., the authors proposed an objective AD severity evaluation metrics – the
78 Eczema Vascular Severity Index (EVSI) using Support Vector Machine (SVM) [18]. Handcrafted
79 skin-specific features derived from RSOM images such as TBV, low-high frequency ratio (LHFR)
80 and ET were used as features to train the model [18]. However, Convolutional Neural Networks
81 (CNNs) were not utilized to automatically extract useful features from 3D RSOM images. In this
82 study, we explore the utilization of CNNs for automatic extraction of useful features from 3D
83 RSOM images and combine these features with handcrafted features proposed by Yew et al. [18].

84 We conducted a comprehensive analysis using three machine learning (ML) methods, SVM,
85 Random Forest (RF) and CNNs in classifying healthy and various AD conditions. We performed
86 two analyses (i) Healthy vs. AD and (ii) Mild vs. Moderate-Severe AD conditions. The
87 motivation for conducting the second analysis in classifying between mild and more serious AD
88 conditions is that patient-specific clinical care can be provided accordingly for better treatment
89 outcomes.

90 To the best of the authors' knowledge, this study is the first effort to employ raw 3D RSOM
91 images for the classification of AD conditions using a deep learning model. The objective of
92 the study is to evaluate the performance of SVM, RF and CNNs in classifying healthy vs. AD
93 conditions and mild vs. moderate-severe AD conditions. We designed an optimal neural network
94 architecture that receives 3D RSOM images and other handcrafted features and successfully
95 combines them in the network.

96 2. Methods and materials

97 2.1. Overview

98 In this study, we performed a thorough analysis by applying three different ML models on 3D
99 RSOM images and compared the performance of each model using different combinations of
100 inputs to the model. We utilized raw 3D RSOM images and four handcrafted features as inputs
101

102

103 to train ML models. Three handcrafted features were derived from RSOM images, proposed by
104 Yew et al. [17], namely TBV, ET and LHFR. The fourth feature is trans-epidermal water loss
105 (TEWL), which reflects skin barrier dysfunction and is shown to be affected in AD condition
106 [28].

107 The workflow of analysis is as follows: First, we evaluated the performance of traditional
108 ML models such as SVM and RF using different combinations of the following features: TBV,
109 ET, LHFR and TEWL. Secondly, we adopted CNN and used raw 3D RSOM images as inputs
110 to train the network. Thirdly, we employed both 3D RSOM images and handcrafted features
111 information to train the CNN model. The performance of models for every combination of inputs
112 was compared and reported.

113

114

2.2. Subjects

115

116

117

118

119

120

121

122

123

124

125

126

127

This study was approved by the Domain Specific Review Board (DSRB) of the National Health Group, Singapore (Ref No. 2017/00932). Patients were imaged in compliance with our institutional approvals and informed consent was obtained. Study participants were recruited from AD patients visiting the National Skin Centre, Singapore. The diagnosis of AD was made based on the Hanifin and Rajka diagnostic criteria [29]. This study also included healthy controls who were defined as not having AD, any form of inflammatory skin diseases and any atopic co-morbidities such as asthma, allergic rhinitis and allergic conjunctivitis. 76 participants were recruited for this study, 53 were AD patients and 23 were healthy controls. All 53 AD participants had their disease severity assessed by an experienced dermatologist using SCORAD. There were 19, 26 and 8 patients suffering from mild, moderate and severe AD, respectively. The criteria of AD severity using SCORAD is as follows: below 25 is defined as mild, between 25 and 50 as moderate and greater than 50 as severe [8].

128

2.3. Image acquisition

129

130

131

132

133

134

135

136

137

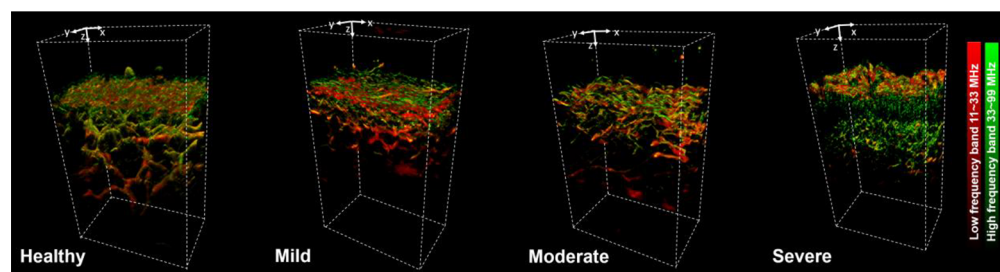
138

139

140

141

The 3D RSOM images were collected by using RSOM Explorer C50 system (iThera Medical GmbH, Germany). RSOM system was implemented with one diode-pumped solid-state (DPSS, Nd:YAG, 532 nm) to provide < 1 ns pulse and a per-pulse energy up to 125 µJ with a laser's repetition rate of 270 Hz. The flexible articulated arm of RSOM allows raster scanning of 5 mm × 3 mm area on the skin in about 2.5 minutes. An in-tandem illumination-detector element is located at the focal point of the transducer, which raster-scans the two-dimensional (2D) region of interest (ROI) on the skin in a regularly-spaced acquisition grid and collects the ultra sound signals from 11 to 99 MHz. This non-invasive RSOM system can provide good quality 3D images with high resolution and deep penetration from the skin surface. The 3D RSOM images were visualized with two frequency sub-bands, high-frequency (HF) (33–99 MHz) in green and low-frequency (LF) (11–33 MHz) in red, representing the small and big vascular structure, respectively (Fig. 1).



151

152

153

Fig. 1. Representative 3D RSOM images for healthy, mild, moderate and severe AD conditions are shown in the figure.

154 2.4. Features

155 In addition to raw voxel values, three handcrafted features extracted from RSOM images and one
156 feature measured using VapoMeter, were used in the evaluation: 1) Total blood volume (TBV),
157 2) Epidermis thickness (ET), 3) The ratio of low and high frequency signals (LHFR) and 4)
158 Transepidermal water loss (TEWL). TEWL was measured using VapoMeter (Delfin Technologies,
159 Kuopio, Finland). TBV, ET and LHFR were extracted from 3D RSOM images using a similar
160 algorithm as described in Li's study [19]. Briefly, TBV was computed as $TBV = \Sigma N \times dV$, where
161 N is the number of pixels with values above a threshold (20% of the maximum value in the
162 dermis region) and dV is a certain voxel's volume. ET was computed as the distance between the
163 skin surface and the melanin layer, which is the basal layer of the epidermis. The melanin layer
164 was detected by averaging pixel-values in the x-y plane along the z-axis and finding the region
165 with overlapping peaks for both high and low frequency optoacoustic profile, representing the
166 center of the melanin layer. The full width at half maximum (FWHM) was performed to obtain
167 the boundary of the melanin layer. LHFR was computed as the ratio of the mean value of the
168 pixels in the LF band image and the HF band image in the dermis region.
169

170 2.5. Machine learning (ML) models

171 Two traditional ML approaches, namely SVM and RF were adopted in classifying (i) healthy
172 vs. AD conditions and (ii) mild AD vs. moderate-severe AD conditions. A linear kernel was
173 employed for the SVM. The RF consists of an ensemble of 25 decision trees, allowed to grow up
174 to a depth of 5 using the entropy criterion. The implementation employed the python library
175 scikit-learn [30]. For both approaches, four features (TBV, ET, LHFR and TEWL) were used
176 as inputs. Features were normalized between 0 and 10. Various combinations of these features
177 were explored to determine the combination that yields the highest accuracy. "Balanced" mode
178 was enabled to account for data balancing during the model training [30]. This mode adjusts the
179 weights given to each sample to be inversely proportional to the class frequency in the training
180 data, which was similar to balancing the data in each severity class during training.
181

182 All the analyses were performed in a six-fold validation fashion. Patients were split into two
183 groups (training and validation) in a stratified manner. Since we had limited datasets, we did not
184 have testing datasets. Therefore, the number of samples used in this ML analysis consists of 53
185 AD and 17 healthy subjects. 80% of patients from each AD severity were assigned as training
186 data and 20% of patients belonging to each AD severity were assigned to validation data.

187 2.6. Deep learning (DL) models

188 2.6.1. Network architecture

189 Our CNN model consists of nine layers as shown in Fig. 2. It is made of five alternating repeated
190 convolutional layers and max-pooling layers followed by five fully-connected (FC) layers to
191 reduce the model complexity [31]. The inputs to the models were 3D LF and HF RSOM images,
192 with a shape of $424 \times 64 \times 64$, stacked together, resulting in a size of $2 \times 424 \times 64 \times 64$. The
193 first layer in the model contains 64 convolutional filters of size $3 \times 3 \times 3$ with a stride of $2 \times 2 \times$
194 2. ReLU (Rectified Linear Unit) activation was applied and was followed by a max-pooling layer
195 as shown below. A softmax was used as the activation function for the output layer.
196

197 We trained two CNN models: (i) using only LF and HF 3D RSOM images (without handcrafted
198 features and (ii) using LF and HF 3D RSOM images with handcrafted features (TBV, ET, LHFR
199 and TEWL). For the second CNN models trained with handcrafted features, the four features
200 were concatenated at the bottleneck layer as shown in Fig. 2. All features were normalized
201 between 0 and 10 to improve CNN model stability and modeling performance.
202

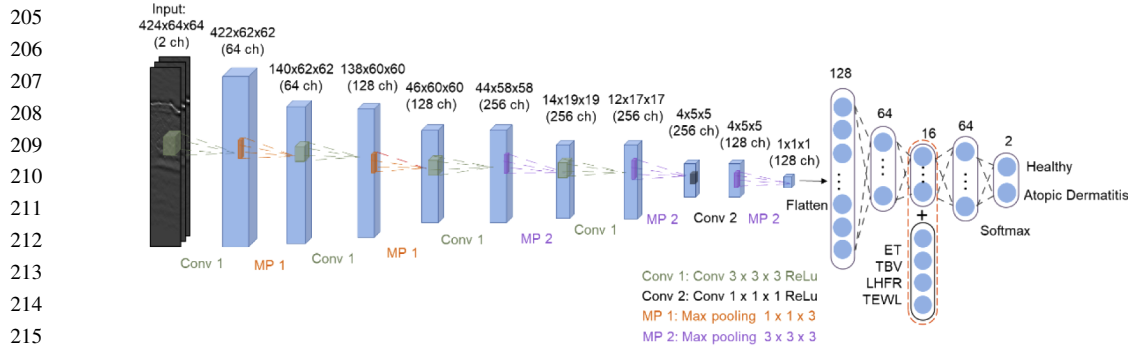


Fig. 2. Figure shows the CNN architecture that was trained to classify 3D RSOM images. Low and high frequency of RSOM images were stacked together, resulting in an input size of $2 \times 424 \times 64 \times 64$. Images underwent a series of convolutional (Conv) and max-pooling (MP) layers for feature extraction. ET (epidermis thickness), TBV (total blood volume), LHFR (low and high frequency ratio), and TEWL (transepidermal water loss) were added at the bottleneck layer.

2.6.2. Data augmentation and balancing

Similar to the ML experiment, CNN analyses were carried out in a six-fold validation fashion. In each fold, data augmentation was performed to balance the data in each severity class. The data augmentation was performed in the training and validation data sets at the patient-level to avoid information leakage [32,33].

The size of 3D RSOM images was $500 \times 150 \times 250$ initially with an axial resolution of $7 \mu\text{m}$ and a lateral resolution of $30 \mu\text{m}$. We first cropped away the blank regions in 3D RSOM images, which did not contain any skin information, resulting in a fixed-size of $424 \times 150 \times 250$. All 3D RSOM images were checked carefully to ensure the resultant cropped 3D RSOM images covered the dermal and epidermal layers. We performed a data augmentation process, as shown in Fig. 3, including flipping (left-right and front-back) and rotating the 3D image stack about the z-axis (45° , 90° , 135° , and 180°). Then, we cropped regions with fixed-size equal to $424 \times 64 \times 64$ pixels from the rotated or flipped images. 64×64 pixels were carefully chosen to include sufficient information for the CNNs model to extract adequate features. Limited by GPU memory, we could only use a cropped region as big as $424 \times 64 \times 64$ pixels in our analysis. This cropping process was repeated until the number of samples in each severity class matched (refers to next paragraph for details). The same cropping was done on both HF and LF images and cropped regions were used as a pair during the training process.

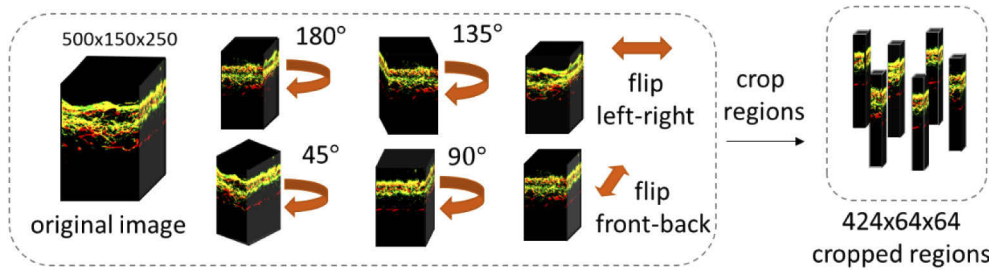


Fig. 3. Data Augmentation Process: To generate a sample, the original 3D RSOM images were rotated about the z-axis or flipped left-right or front-back and a small region of fixed size $424 \times 64 \times 64$ was randomly cropped from the rotated or flipped image.

Tables 1 and 2 show the number of cropped regions per patient for one of the cross-validation datasets using 3D RSOM images as input to train the model (23 healthy and 53 AD patients). In the healthy vs. AD analysis, we performed data augmentation and balancing as described above until we had ~200 training samples and ~20 validation samples in each severity class. For example, in Table 1, we have 15 mild AD patients, five regions were randomly cropped after rotating and flipping the patient's HF and LF 3D RSOM images giving a total of 75 cropped regions for the mild category. A similar number of regions were augmented for patients with moderate and severe AD conditions giving a total of 210 augmented regions for AD condition (mild, moderate and severe classes), which were comparable to the total number of augmented regions for the healthy subjects (209 regions). Similar data augmentation was performed for validation data and mild vs. moderate-severe analyses. The details of the total number of regions cropped are shown in Table 2.

Table 1. Table shows the number of subjects in the experiment of healthy vs atopic dermatitis, the number of cropped regions per subject and total number of samples generated at the end of the augmentation process (stated in the total number of cropped regions column) for training and validation data sets. The table shows one of the cross-validation fold.

Healthy vs. Atopic Dermatitis Analysis						
Severity	Training Data			Validation Data		
	Num. of Subjects	Num. of Cropped Regions per Subject	Total Num. of Cropped Regions	Num. of Subjects	Num. of Cropped Regions per Subject	Total Num. of Cropped Regions
Mild	15	5	75	4	1	4
Moderate	20	3	60	6	1	6
Severe	6	12	72	2	1	6
Healthy	19	11	209	4	5	20

Table 2. Table shows the number of patients in the experiment of mild vs moderate-severe, the number of cropped regions per patient and total number of samples generated at the end of the augmentation process (stated in the total number of cropped regions column) for training and validation data sets. The table shows one of the cross-validation fold.

Mild vs. Moderate-Severe Analysis						
Severity	Training Data			Validation Data		
	Num. of Patients	Num. of Cropped Regions per Patients	Total Num. of Cropped Regions	Num. of Patients	Num. of Cropped Regions per Patients	Total Num. of Cropped Regions
Mild	15	5	225	4	5	20
Moderate	20	5	100	6	2	12
Severe	6	18	108	2	5	10

2.6.3. Model training and evaluation

The network was trained for 200 epochs with learning rate 1×10^{-5} , learning rate decay of 0.05 and learning step decay of two with Adam optimizer. The batch size was set to be four. All computations were carried out on a Linux workstation with Intel Core i7-4790 CPU with 3.6 GHz clock speed, 16 GB RAM and a GeForce GTX TITAN X. It took approximately 9 min for one epoch and a total of 30 hours to train the model using the above-mentioned workstation. Tensorflow 1.12 [34] implementation was used in our study. Three CNN models were trained using different combinations of inputs.

The first CNN model trained used only LF and HF 3D RSOM images (23 healthy and 53 AD cases) as inputs. The second CNN model trained used 3D RSOM images, and three features

(TBV, LHFR, and TEWL) added at the bottleneck layer (Fig. 2). The third CNN model used 3D RSOM images and four features (ET, TBV, LHFR, and TEWL). For the second and third analyses, 6 cases out of the 23 healthy cases did not have complete feature information, making the number of samples to be 53 AD and 17 healthy cases. Validation data was used to evaluate the models' prediction accuracy. Since one patient would have more than one sample due to the cropping pipeline, majority voting was performed to determine the final prediction for that patient. If there is a patient without a final prediction due to having an equal number of prediction outcomes, one additional sample was randomly cropped from the 3D RSOM images and evaluated to obtain the final prediction.

3. Results

Table 3 tabulates the average and standard deviation of the validation accuracy of RF, SVM and CNN for six-fold cross-validation results. Figure 4 shows the confusion matrices for the three models evaluated on validation datasets. The confusion matrices shown are for models that yielded the highest validation accuracy as reported in Table 3.

Table 3. Validation accuracy for two analyses using three models with specified inputs to the models. Values shown are average and standard deviation for six-fold cross-validation. The highest validation accuracy for each particular model is shown in bold. TBV: Total Blood Volume, LHFR: Low High Frequency Ratio, ET: Epidermis Thickness, TEWL: Transepidermal water loss measured from VapoMeter.

Model	Inputs to Model				Validation Accuracy	
	3D RSOM	Features derived from RSOM			TEWL	Healthy vs. Atopic Dermatitis
		TBV	LHFR	ET		Mild vs. Moderate-Severe
RF		✓	✓	✓	✓	0.81 ± 0.08
		✓	✓	✓		0.92 ± 0.07
		✓	✓			0.91 ± 0.06
SVM		✓	✓	✓	✓	0.77 ± 0.08
		✓	✓	✓		0.82 ± 0.11
		✓	✓			0.86 ± 0.10
CNN	✓				✓	0.48 ± 0.13
		✓	✓	✓		0.94 ± 0.10
		✓	✓	✓		0.97 ± 0.04

In healthy vs. AD analysis, CNN achieved the highest performance among the three models, giving a validation accuracy of 97%, using all four features. However, when using only LF and HF 3D RSOM images, CNN yielded only 48% validation accuracy in classifying healthy vs. AD condition. Adding three handcrafted features (TBV, LHFR and ET) to the model increased the validation accuracy to 94%. The performance of CNN was further improved by 3% when TEWL was added to the model, achieving 97% accuracy. For ML models, RF performed better than SVM in all the analyses performed for different combinations of features.

In mild vs. moderate-severe analysis, RF gave the highest accuracy of 65% in severity score prediction among all three models using all four features. SVM model, on the other hand, showed a validation accuracy of 59% when TBV, LHFR, and ET were used. Lastly, CNN exhibited slightly lower accuracy at 56% in predicting severity compared to RF and SVM, using 3D RSOM images and three handcrafted features derived (TBV, LHFR, ET) from RSOM images as inputs.

Figure 5 shows the representative RSOM images that were correctly and wrongly classified by CNN in the analyses of healthy vs. AD conditions. While the structural differences between healthy and AD conditions are apparent, the moderate AD condition that was wrongly classified

358

359

360

361

362

363

364

365

366

a) (i) RF: Healthy vs Atopic Dermatitis

		Prediction	
		Healthy	Eczema
Ground Truth	Healthy	3.0 ± 0.6	0.3 ± 0.5
	Eczema	0.7 ± 0.9	9.0 ± 0.8

Inputs : TBV + LHFR + ET + TEWL**Accuracy : 0.92 ± 0.07****b) (i) SVM: Healthy vs Atopic Dermatitis**

		Prediction	
		Healthy	Eczema
Ground Truth	Healthy	3.2 ± 0.4	0.2 ± 0.4
	Eczema	1.7 ± 1.1	8.0 ± 1.1

Inputs : TBV + LHFR + TEWL**Accuracy : 0.86 ± 0.10****c) (i) CNN: Healthy vs Atopic Dermatitis**

		Prediction	
		Healthy	Eczema
Ground Truth	Healthy	3.3 ± 0.5	0.0 ± 0.0
	Eczema	0.3 ± 0.5	9.3 ± 0.8

Inputs : RSOM + TBV + LHFR + ET + TEWL**Accuracy : 0.97 ± 0.04****a) (ii) RF: Mild vs Moderate-Severe**

		Prediction	
		Mild	Mod-Sev
Ground Truth	Mild	1.3 ± 0.9	1.8 ± 0.7
	Mod-Sev	1.2 ± 0.7	4.5 ± 1.0

Inputs : TBV + LHFR + ET + TEWL**Accuracy : 0.65 ± 0.09****b) (ii) SVM: Mild vs Moderate-Severe**

		Prediction	
		Mild	Mod-Sev
Ground Truth	Mild	2.3 ± 0.5	0.8 ± 0.4
	Mod-Sev	2.8 ± 1.3	2.8 ± 1.1

Inputs : TBV + LHFR + ET**Accuracy : 0.59 ± 0.12****c) (ii) CNN: Mild vs Moderate-Severe**

		Prediction	
		Mild	Mod-Sev
Ground Truth	Mild	2.3 ± 0.8	0.8 ± 0.8
	Mod-Sev	3.0 ± 0.9	2.7 ± 1.4

Inputs : RSOM + TBV + LHFR + ET**Accuracy : 0.56 ± 0.17**

Fig. 4. Confusion Matrix for all models in the two analyses. The confusion matrices shown is generated using the model that yielded the highest validation accuracy as reported in Table 3. Values shown are mean and standard deviation for six-fold cross-validations. Inputs are the images/features used to train the model. RF: Random Forest, SVM: Support Vector Machine, CNN: Convolutional Neural Networks, TBV: Total Blood Volume, LHFR: Low High Frequency Ratio, ET: Epidermis Thickness, TEWL: Transepidermal Water Loss.

as healthy may have similar structural features to the healthy case, such as the absence of capillary loops, and intact epidermis. Figure 6 shows the representative RSOM images that were wrongly classified by CNN in the analysis of mild vs. moderate-severe AD conditions. In other words, the mild AD case was classified as a moderate-severe AD case and vice versa.

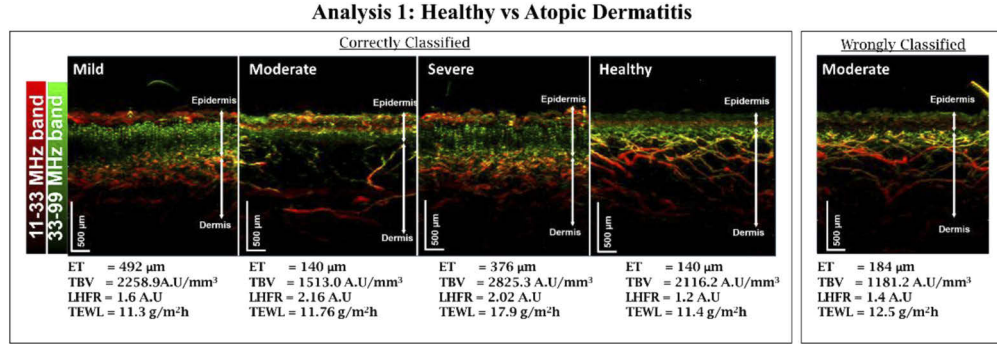


Fig. 5. Representative RSOM cross-sectional images of correctly and wrongly classified by CNN in the experiment of classifying healthy vs. AD condition.

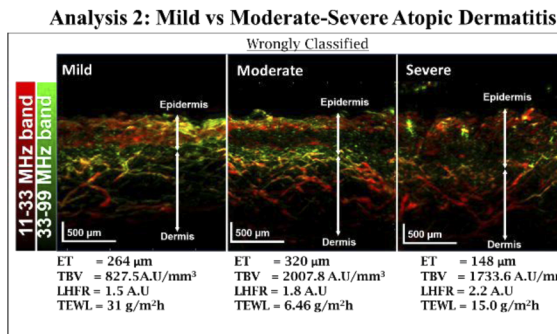


Fig. 6. Representative RSOM cross-sectional images of wrongly classified samples by the CNN in the experiment of classifying mild vs. non-mild AD (moderate-severe) conditions.

4. Discussion

In recent years, there have been a number of studies deploying deep learning for skin disease classification. These studies applied deep learning on dermoscopic images [26,35,36] but not on 3D optoacoustic images. In this paper, we deploy deep learning for classification of 3D RSOM images.

Using a small data set (76 patients), we could achieve a better diagnostic accuracy compared to the model by Liu et al. which was trained on a large data set (~16 k dermoscopic images) [37]. Using RSOM images, we were able to boost the model's performance with a smaller data set. These results suggested that the ML model's performance could be largely affected by the data information presented to the model. As data labeling is a laborious task for preparing large data sets of medical imaging for ML, highly efficient models on small data sets can be a boon in timely analyses [38–40].

We extended our work based on previous studies on RSOM image analysis. In the current study, we adopted the ML model to classify different AD severity conditions – mild vs. moderate-severe condition, which was not performed in the past. Furthermore, we performed comprehensive ML

460 training and predictive validation analyses, where we did cross-validation for the generalization of
461 our model. It is particularly important to obtain more reliable results especially when the datasets
462 are small. Our cross-validation results showed that CNNs had higher prediction accuracies than
463 RF and SVM, with an accuracy of 97%, achieving 11% improvement over SVM, in classifying
464 healthy and AD conditions [18].

465 Using all four handcrafted features, traditional ML models such as RF and SVM could achieve
466 a diagnostic accuracy of 92% and 86% in classifying healthy and AD condition, respectively
467 (refers to Table 3). When raw 3D RSOM images were added to the pipeline using CNN, the
468 diagnostic accuracy was improved to 97% and the model demonstrated more stability in prediction
469 compared to RF and SVM, judging from the low standard deviation. This suggested that the
470 CNN model indeed extracted useful features from 3D RSOM images, which aided in enhancing
471 the CNN's diagnostic accuracy. Even though CNN showed very high diagnostic accuracy in
472 classifying healthy and AD conditions, it did not achieve similar performance in classifying
473 mild vs. moderate-severe AD conditions. The CNN's highest diagnostic accuracy for mild vs
474 moderate-severe AD classification was 56%. A similar prediction accuracy was observed in RF
475 and SVM, where the average diagnostic accuracy was ~60%.

476 From Fig. 5, the RSOM cross-sectional images for healthy and AD cases were visibly
477 distinguishable. CNN model thus was able to extract useful features in classifying healthy and
478 AD cases even though the datasets were small. For the mild vs. moderate-severe AD conditions,
479 using both raw 3D RSOM images and handcrafted features did not improve the CNN model's
480 accuracy as what we had observed in the healthy vs. AD classification. We believe this was
481 because it is challenging to differentiate between mild and moderate-severe AD RSOM images,
482 as shown in Figs. 5 and 6. There are several reasons for the erroneous classification in Fig. 6.
483 Firstly, since pathological and physiological features form the basis for determining the severity
484 of AD in this study, any deviation in the features will affect the CNN's prediction accuracy.
485 Notably, the mild representative case in Fig. 6 exhibited a TEWL value of 31 g/m²h, far higher
486 than that of severe AD cases. Similarly, the TEWL value of the moderate representative case
487 in Fig. 6 was lower than that of healthy subjects, possibly rendering the wrong classification
488 of the case to be 'mild'. Secondly, if the structural features of the RSOM images are lost due
489 to skin barrier dysfunction in severe AD cases, the feature quantification is challenging since
490 the boundary between epidermis and dermis region is not delineated. As in the severe case in
491 Fig. 6, the ET calculation yields a value of 148 μm, similar to that of healthy subjects which
492 leads it to be wrongly classified. The limited amount of training data further adds to the difficulty
493 resulting in inaccurate classification for validation data set. As discussed, there are a total of
494 41 AD and 19 healthy subjects in our data set for classifying healthy vs AD cases. However, to
495 predict mild vs moderate-severe AD subjects, fewer samples are available including 15 mild AD
496 subjects and 26 moderate-severe AD subjects. The limited number of samples is another reason
497 for why classification of mild AD vs moderate-severe AD subjects is harder. CNN models in
498 general require many more samples in order to learn to extract useful features for classification.
499 Retraining the model with a larger data set will mitigate this problem.

500 During ML training, data balance between classes (e.g. healthy vs. disease) is important
501 to ensure the number of samples from both classes is similar. It is particularly important to
502 perform data splitting at the patients-level to avoid potential data leakage from training data to
503 validation data [37]. We have successfully developed a CNN-based pipeline, which include data
504 preparation, data augmentation and model training to recognize various AD severity conditions
505 using raw 3D RSOM images, and handcrafted features. This CNN-based pipeline thus will
506 handle the data splitting at patient-level and is not limited only to skin AD disease classification.
507 It is designed in a modularized manner and has the flexibility to be applied for classification of
508 other skin inflammatory diseases such as rosacea, and psoriasis and other 3D optoacoustic images
509 such as optical coherence tomography, multispectral optoacoustic tomography and multispectral
510

511 optoacoustic mesoscopy. We have shared our code in <https://github.com/davidc9320sg/rsom-dermatitis-cnn/>.
512

513 It is crucial to diagnose AD severity accurately to monitor the treatment response and plan
514 effective clinical care for patients. We successfully proposed an optimal network architecture
515 suitable for 3D optoacoustic images for AD conditions classification, which can be used as an
516 objective evaluation tool for assessing AD conditions in clinics. At the current state, our CNN
517 model is unable to achieve desirable diagnostic accuracy in classifying mild vs. moderate-severe
518 AD conditions. One reason could be that the AD severities were determined from SCORAD
519 scoring which was subjected to inter- and intra-observational variability, the accuracy may
520 therefore suffer from discrepancies from the SCORAD results. While SCORAD or EASI takes
521 into account the presentation and frequency of AD symptoms, the subsurface inflammation
522 physiology of the skin was out of the scoring framework. With the naked eye, it may be possible
523 to observe that superficial symptoms are improved overtime with treatment, but inflammation
524 may persist under the skin that can significantly impact the way we classify the disease severity.
525 With more data collected and consensus among multiple diagnoses for each patient, the model
526 can be re-trained using the current framework as a baseline to further enhance its accuracy.
527

528 There are several limitations in this study. Firstly, the size of the data set was small (76 patients)
529 and the population was mainly Asian cohort. Through an on-going collaboration, we are aiming
530 to expand this study by including patients with lower Fitzpatrick scores (I-II). Secondly, the size
531 of the cropped sample was set at 64×64 pixels due to our insufficient GPU memory. A larger
532 cropped sample might aid in improving CNN models since it provides more information to the
533 CNN model.

534 The AD classification model in this paper can be an adjunctive diagnostic tool to aid in
535 clinical decisions, especially in differentiating between mild and non-mild AD severities. As
536 even clinicians with experience in optoacoustic images may face challenges to interpret the
537 RSOM images, our classification model aims to classify AD severity with higher sensitivity by
538 extracting features from volumetric vascular structure in 3D RSOM images rather than one-plane
539 imaging features. This proposed pipeline provides the foundation for an AI-aided AD diagnosis
540 and treatment platform.

541 5. Conclusion

542 To conclude, we have evaluated the performance of three ML models in classifying AD conditions
543 using 3D RSOM images, handcrafted features derived from RSOM images and transepidermal
544 water loss. Our results showed that CNN models yield the highest accuracy (97%) in classifying
545 healthy vs. AD conditions while RF achieve the highest accuracy (65%) in classifying mild vs.
546 moderate-severe AD conditions. This is the first study to classify AD severity using 3D RSOM
547 images. We developed a pipeline to prepare 3D RSOM images for training a CNN model and
548 showed that the use of raw RSOM voxel values can be advantageous over handcrafted features.
549 Our method can easily be extended to other inflammatory skin diseases such as rosacea and
550 psoriasis.

551 **Funding.** Biomedical Research Council; National Medical Research Council (NMRC OF-IRG Grant OFIRG18nov-0101).

Q1

552 **Acknowledgment.** Acknowledgement also goes to SBIC-iThera joint lab for their help in this study.

553 **Disclosures.** The authors declare no conflicts of interest.

554 555 References

1. J. I. Silverberg and J. M. Hanifin, "Adult eczema prevalence and associations with asthma and other health and demographic factors: A US population-based study," *J. Allergy Clin. Immunol.* **132**(5), 1132–1138 (2013).
2. G. Pesce, A. Marcon, A. Carosso, L. Antonicelli, L. Cazzoletti, M. Ferrari, A. G. Fois, P. Marchetti, M. Olivieri, P. Pirina, G. Pocetta, R. Tassinari, G. Verlato, S. Villani, and R. de Marco, "Adult eczema in Italy: prevalence and associations with environmental factors," *J Eur Acad Dermatol Venereol* **29**(6), 1180–1187 (2015).

- 562 3. Y. I. Lopez Carrera, A. Al Hammadi, Y.-H. Huang, L. J. Llamado, E. Mahgoub, and A. M. Tallman, "Epidemiology,
563 Diagnosis, and Treatment of Atopic Dermatitis in the Developing Countries of Asia, Africa, Latin America, and the
564 Middle East: A Review," *Dermatol Ther (Heidelb)* **9**(4), 685–705 (2019).
- 565 4. C. Hoare, A. Li Wan Po, and H. Williams, "Systematic review of treatments for atopic eczema," *Health Technology
Assessment* **4**, 1–191 (2000).
- 566 5. F. S. Larsen, N. V. Holm, and K. Henningsen, "Atopic dermatitis. A genetic-epidemiologic study in a population-based
567 twin sample," *J. Am. Acad. Dermatol.* **15**(3), 487–494 (1986).
- 568 6. Q. Deng, C. Lu, Y. Li, J. Sundell, and N. Dan, "Exposure to outdoor air pollution during trimesters of pregnancy and
childhood asthma, allergic rhinitis, and eczema," *Environ. Res.* **150**, 119–127 (2016).
- 569 7. W. David Boothe, J. A. Tarbox, and M. B. Tarbox, "Atopic Dermatitis: Pathophysiology," in *Management of Atopic
Dermatitis: Methods and Challenges*, E. A. Fortson, S. R. Feldman, and L. C. Strowd, eds. (Springer International
Publishing, 2017), pp. 21–37.
- 570 8. R. Chopra, P. Vakharia, R. Sacotte, N. Patel, S. Immaneni, T. White, R. Kantor, D. Hsu, and J. Silverberg, "Severity
571 strata for Eczema Area and Severity Index (EASI), modified EASI, Scoring Atopic Dermatitis (SCORAD), objective
SCORAD, Atopic Dermatitis Severity Index and body surface area in adolescents and adults with atopic dermatitis,"
Br. J. Dermatol. **177**(5), 1316–1321 (2017).
- 572 9. P. P. Vakharia, R. Chopra, R. Sacotte, N. Patel, S. Immaneni, T. White, R. Kantor, D. Y. Hsu, and J. I. Silverberg,
573 "Validation of patient-reported global severity of atopic dermatitis in adults," *Allergy* **73**(2), 451–458 (2018).
- 574 10. Y. Leshem, T. Hajar, J. Hanifin, and E. Simpson, "What the Eczema Area and Severity Index score tells us about the
severity of atopic dermatitis: an interpretability study," *Br. J. Dermatol.* **172**(5), 1353–1357 (2015).
- 575 11. C. R. Charman, A. J. Venn, H. Williams, and M. Bigby, "Measuring atopic eczema severity visually: which variables
576 are most important to patients?" *Arch. Dermatol.* **141**(9), 1146–1151 (2005).
- 577 12. A. Bożek and A. Reich, "Assessment of intra-and inter-rater reliability of three methods for measuring atopic
dermatitis severity: EASI, objective SCORAD, and IGA," *Dermatology* **233**(1), 16–22 (2017).
- 578 13. M. Omar, J. Gateau, and V. Ntziachristos, "Raster-scan optoacoustic mesoscopy in the 25–125 MHz range," *Opt. Lett.*
579 **38**(14), 2472–2474 (2013).
- 580 14. J. Aguirre, M. Schwarz, N. Garzor, M. Omar, A. Buehler, K. Eyerich, and V. Ntziachristos, "Precision assessment of
581 label-free psoriasis biomarkers with ultra-broadband optoacoustic mesoscopy," *Nat. Biomed. Eng.* **1**(5), 0068 (2017).
- 582 15. B. Hindelang, J. Aguirre, A. Berezhnoi, T. Biedermann, U. Darsow, B. Eberlein, and V. Ntziachristos, "Quantification
583 of skin sensitivity to ultraviolet radiation using ultra-wideband optoacoustic mesoscopy," *Br. J. Dermatol.* (2020).
- 584 16. B. Hindelang, J. Aguirre, A. Berezhnoi, H. He, K. Eyerich, V. Ntziachristos, T. Biedermann, and U. Darsow,
585 "Optoacoustic mesoscopy shows potential to increase accuracy of allergy patch testing," *Contact Dermatitis* (2020).
- 586 17. C. Avena-Woods, "Overview of atopic dermatitis," *Am. J. Manag. Care* **23**, S115–S123 (2017).
- 587 18. Y. W. Yew, U. Dinish, A. H. Y. Kuan, X. Li, K. Dev, A. B. E. Attia, R. Bi, M. Moothanchery, G. Balasundaram, and J.
588 Aguirre, "Raster-scanning optoacoustic mesoscopy (RSOM) imaging as an objective disease severity tool in atopic
589 dermatitis patients," *J. Am. Acad. Dermatol.* (2020).
- 590 19. X. Li, U. Dinish, J. Aguirre, R. Bi, K. Dev, A. B. E. Attia, S. Nitkunanantharajah, Q. H. Lim, M. Schwarz, and Y. W.
591 Yew, "Optoacoustic mesoscopy analysis and quantitative estimation of specific imaging metrics in Fitzpatrick skin
592 phototypes II to V," *J. Biophotonics* **12**, e201800442 (2019).
- 593 20. Y. Fujisawa, Y. Otomo, Y. Ogata, Y. Nakamura, R. Fujita, Y. Ishitsuka, R. Watanabe, N. Okiyama, K. Ohara, and
594 M. Fujimoto, "Deep-learning-based, computer-aided classifier developed with a small dataset of clinical images
595 surpasses board-certified dermatologists in skin tumour diagnosis," *Br. J. Dermatol.* **180**(2), 373–381 (2019).
- 596 21. J. Premaladha and K. S. Ravichandran, "Novel approaches for diagnosing melanoma skin lesions through supervised
597 and deep learning algorithms," *J Med Syst* **40**(4), 96 (2016).
- 598 22. A. Esteva, B. Kuprel, R. A. Novoa, J. Ko, S. M. Swetter, H. M. Blau, and S. Thrun, "Dermatologist-level classification
599 of skin cancer with deep neural networks," *Nature* **542**(7639), 115–118 (2017).
- 600 23. A. Rezvantalab, H. Safigholi, and S. Karimijeshni, "Dermatologist level dermoscopy skin cancer classification using
601 different deep learning convolutional neural networks algorithms," arXiv preprint arXiv:1810.10348 (2018).
- 602 24. S. S. Han, M. S. Kim, W. Lim, G. H. Park, I. Park, and S. E. Chang, "Classification of the clinical images for benign
603 and malignant cutaneous tumors using a deep learning algorithm," *J. Invest. Dermatol.* **138**(7), 1529–1538 (2018).
- 604 25. E. Nasr-Esfahani, S. Samavi, N. Karimi, S. M. R. Soroushmehr, M. H. Jafari, K. Ward, and K. Najarian, "Melanoma
605 detection by analysis of clinical images using convolutional neural network," in *2016 38th Annual International
Conference of the IEEE Engineering in Medicine and Biology Society (EMBC)*(2016), pp. 1373–1376.
- 606 26. S.-Q. Wang, X.-Y. Zhang, J. Liu, C. Tao, C.-Y. Zhu, C. Shu, T. Xu, and H.-Z. Jin, "Deep learning-based, computer-aided
607 classifier developed with dermoscopic images shows comparable performance to 164 dermatologists in cutaneous
608 disease diagnosis in the Chinese population," *Chin Med J (Engl)* **133**(17), 2027–2036 (2020).
- 609 27. A. Minagawa, H. Koga, T. Sano, K. Matsunaga, Y. Teshima, A. Hamada, Y. Houjou, and R. Okuyama, "Dermoscopic
610 diagnostic performance of Japanese dermatologists for skin tumors differs by patient origin: A deep learning
611 convolutional neural network closes the gap," *The Journal of Dermatology* n/a.
- 612 28. S. G. Danby and M. J. Cork, "The skin barrier in atopic dermatitis," *Curr Allergy Asthma Rep* **14**(5), 433 (2014).
- 613 29. Y. W. Yew, U. Dinish, E. C. E. Choi, R. Bi, C. J. H. Ho, K. Dev, X. Li, A. B. E. Attia, M. K. W. Wong, and G.
Balasundaram, "Investigation of morphological, vascular and biochemical changes in the skin of an atopic dermatitis

- 613 (AD) patient in response to dupilumab using raster scanning optoacoustic mesoscopy (RSOM) and handheld confocal
614 Raman spectroscopy (CRS)," *J. Dermatol. Sci.* **95**(3), 123–125 (2019).
- 615 30. F. Pedregosa, G. Varoquaux, A. Gramfort, V. Michel, B. Thirion, O. Grisel, M. Blondel, P. Prettenhofer, R. Weiss, and
616 V. Dubourg, "Scikit-learn: Machine learning in Python," the Journal of machine Learning research **12**, 2825–2830
(2011).
- 617 31. Z. Lin, R. Memisevic, and K. Konda, "How far can we go without convolution: Improving fully-connected networks,"
618 arXiv preprint arXiv:1511.02580 (2015).
- 619 32. N. Bussola, A. Marcolini, V. Maggio, G. Jurman, and C. Furlanello, "Not again! Data leakage in digital pathology,"
arXiv preprint arXiv:1909.06539 (2019).
- 620 33. L. Shi, G. Campbell, W. Jones, F. Campagne, Z. Wen, S. Walker, Z. Su, T. Chu, F. Goodsaid, and L. Pusztai, "The
621 MAQC-II project: a comprehensive study of common practices for the development and validation of microarray-based
622 predictive models," (2010).
- 623 34. M. Abadi, P. Barham, J. Chen, Z. Chen, A. Davis, J. Dean, M. Devin, S. Ghemawat, G. Irving, and M. Isard,
"Tensorflow: A system for large-scale machine learning," in *12th {USENIX} symposium on operating systems design
and implementation ({OSDI} 16)*(2016), pp. 265–283.
- 625 35. S. Jinnai, N. Yamazaki, Y. Hirano, Y. Sugawara, Y. Ohe, and R. Hamamoto, "The development of a skin cancer
626 classification system for pigmented skin lesions using deep learning," *Biomolecules* **10**(8), 1123 (2020).
- 627 36. A. Minagawa, H. Koga, T. Sano, K. Matsunaga, Y. Teshima, A. Hamada, Y. Houjou, and R. Okuyama, "Dermoscopic
628 diagnostic performance of Japanese dermatologists for skin tumors differs by patient origin: a deep learning
convolutional neural network closes the gap," *The Journal of Dermatology* n/a (2020).
- 629 37. Y. Liu, A. Jain, C. Eng, D. H. Way, K. Lee, P. Bui, K. Kanada, G. de Oliveira Marinho, J. Gallegos, S. Gabriele, V.
630 Gupta, N. Singh, V. Natarajan, R. Hofmann-Wellenhof, G. S. Corrado, L. H. Peng, D. R. Webster, D. Ai, S. J. Huang,
Y. Liu, R. C. Dunn, and D. Coz, "A deep learning system for differential diagnosis of skin diseases," *Nat. Med.* **26**(6),
900–908 (2020).
- 632 38. N. Tajbakhsh, L. Jeyaseelan, Q. Li, J. N. Chiang, Z. Wu, and X. Ding, "Embracing imperfect datasets: a review of
633 deep learning solutions for medical image segmentation," *Med. Image Anal.* **63**, 101693 (2020).
- 634 39. G. Zhang, C.-H. R. Hsu, H. Lai, and X. Zheng, "Deep learning based feature representation for automated skin
histopathological image annotation," *Multimed Tools Appl* **77**(8), 9849–9869 (2018).
- 635 40. D. C. Castro, I. Walker, and B. Glocker, "Causality matters in medical imaging," *Nat. Commun.* **11**(1), 3673 (2020).
- 636
- 637
- 638
- 639
- 640
- 641
- 642
- 643
- 644
- 645
- 646
- 647
- 648
- 649
- 650
- 651
- 652
- 653
- 654
- 655
- 656
- 657
- 658
- 659
- 660
- 661
- 662
- 663